ARTICLE

A new easy method for determination of surface adhesion of phototrophic biofilms

Judith Stiefelmaier[1] | Dorina Strieth[1] | Susanne Schaefer[2] | Björn Wrabl[1] | Daniel Kronenberger[1] | Ulrich Bröckel[2] | Roland Ulber[1]

[1]RPTU Kaiserslautern-Landau, Institute of Bioprocess Engineering, Kaiserslautern, Germany

[2]Environmental Campus Birkenfeld, Institute of Microprocess Engineering and Particle Technology, University of Applied Sciences Trier, Birkenfeld, Germany

Correspondence
Roland Ulber, RPTU Kaiserslautern-Landau, Institute of Bioprocess Engineering, Gottlieb-Daimler-Str. 49, 67663 Kaiserslautern, Germany.
Email: ulber@mv.uni-kl.de

Abstract

Terrestrial cyanobacteria grow as phototrophic biofilms and offer a wide spectrum of interesting products. For cultivation of phototrophic biofilms different reactor concepts have been developed in the last years. One of the main influencing factors is the surface material and the adhesion strength of the chosen production strain. In this work a flow chamber was developed, in which, in combination with optical coherence tomography and computational fluid dynamics simulation, an easy analysis of adhesion forces between different biofilms and varied surface materials is possible. Hereby, differences between two cyanobacteria strains and two surface materials were shown. With longer cultivation time of biofilms adhesion increased in all experiments. Additionally, the content of extracellular polymeric substances was analyzed and its role in surface adhesion was evaluated. To test the comparability of obtained results from the flow chamber with other methods, analogous experiments were conducted with a rotational rheometer, which proved to be successful. Thus, with the presented flow chamber an easy to implement method for analysis of biofilm adhesion was developed, which can be used in future research for determination of suitable combinations of microorganisms with cultivation surfaces on lab scale in advance of larger processes.

KEYWORDS
adhesion, flow chamber, optical coherence tomography, phototrophic biofilms, rotational rheometer

1 | INTRODUCTION

1.1 | Cyanobacteria and biofilm adhesion

With an occurrence since 2.7–2.8 billion years cyanobacteria belong to the oldest known microorganisms (Hedges et al., 2001), which played an important role in formation of the atmosphere, due to their ability of oxygenic photosynthesis (Schirrmeister et al., 2015). Attributable to their different pigments, which find already application as natural colorants in food or cosmetic industries (Kuddus et al., 2013), various pharmaceutically interesting substances (Fleming & Castenholz, 2007; Swain et al., 2017) and their nutrient rich biomass (Castillejo et al., 2018; Lupatini et al., 2017), which makes them a good dietary supplement, cyanobacteria are an increasing field of research and production

processes. Depending on the habitat, aquatic and terrestrial cyanobacteria are distinguished (Garcia-Pichel et al., 2003). Terrestrial cyanobacteria thereby grow attached to surfaces, such as rocks, trees, or on the soil in form of biofilms. Cells are living embedded in a matrix of self-produced extracellular polymeric substances (EPS), which contains, besides water, polysaccharides, proteins, fatty acids, and nucleic acids (Flemming & Wingender, 2010). The EPS possess different important functions such as nutrient storage or protection from drought (Stuart et al., 2016; Tamaru et al., 2005). Furthermore, EPS have a key role in adhesion to surfaces and thus development of biofilms (Carniello et al., 2018). In biofilm formation on surfaces different phases can be distinguished: (I) the conditioning of the surface, (II) the attachment of few cells, (III) the reversible adhesion and (IV) the irreversible adhesion to the surface, (V) growth of the biofilm, (VI) stationary phase, and (VII) the death phase or the detachment of individual cells or biofilm fragments to colonize new surfaces (Bryers & Ratner, 2004; Carniello et al., 2018). Hereby, in phase (III) and (IV) EPS production is increased. The adhesion is influenced by different surface properties such as hydrophobicity, roughness, topography, or charge, which was summarized by Song et al. (2015).

1.2 | Influence of adhesion strength on biofilm cultivation

For the cultivation of cyanobacteria and other microalgae in biofilms, different reactor concepts have been developed in the last years, such as exemplarily aerosol photobioreactors (Scherer et al., 2020; Strieth et al., 2021), rotating disc reactors (Blanken et al., 2014), or porous substrate photobioreactors (Murphy & Berberoglu, 2014). Hereby, one important parameter is the adhesion of the biofilm to the cultivation surface, whereby requirements differ between different cultivation systems. During cultivation strong adhesion is helpful, preventing detachment and loss of biomass. Especially in continuous processes as described by Li et al. (2015) a strong adhesion is advantageous. For processes with harvesting of biomass at the end, weaker adhesion simplifies harvesting, so adhesion should only be strong enough to prevent biofilm detachment during cultivation. Another process strategy, in which sufficient adhesion is necessary, are semicontinuous processes as for example described by Strieth et al. (2017). Here, cycles of biofilm cultivation alternate with addition of an extraction solution for EPS extraction. After extraction, the biofilm needs to remain attached to the surface for resumption of the next cycle of biofilm cultivation. Additionally, the controlled attachment to cultivation surfaces only, and not for example the overgrowth of reactor installations such as sensors, is a challenging task (Sweity et al., 2011).

1.3 | Methods for examination of biofilm adhesion

Since adhesion is strain specific and as well depends on surface material and structure (summarized by Song et al., 2015), methods for the easy examination of suitability of cyanobacteria strains in combination with surface materials for a distinct cultivation setup are necessary. Hereby, the examination of adhesion forces of single cells and of complete biofilms can be distinguished. Single cell adhesion can be analyzed by scanning force microscopy, which allows to draw conclusions about the first steps of biofilm formation (Davoudi et al., 2017; Huttenlochner et al., 2018). For detection of adhesion forces of complete biofilms different developments have already been described. Thereby, shear forces were applied by cultivating in a rotating cylinder (Hassan et al., 2012), by introduction of an increasing pump speed in an overgrown rectangular flow cell, by centrifugation of surfaces grown over with biofilm (Ohashi & Harada, 1994) or by pumping of liquid through channels (height <1 mm) with biofilm in a PDMS flow chamber (Kozuka et al., 2021; Ozkan & Berberoglu, 2013). Another possibility is the use of a rotational rheometer, which usually finds application in materials science, but as well is described for the examination of biofilm characteristics (Houari et al., 2008; Towler et al., 2003).

For use as a preliminary investigation on a laboratory scale before scaling up cultivation processes, an easy-to-implement method for the rapid analysis of different surface materials with diverse biofilms would be beneficial. Since phototrophic biofilms have rather low growth rates, cultivation in an application separate from the adhesion analysis system is preferable to allow measurement of replicates in a short time. Separating the adhesion study from the cultivation system also makes it possible to evaluate the adhesion strength that a biofilm develops under the prevailing conditions in the cultivation system that will be used in the subsequent process.

As a possibility for easy adhesion studies, in this work a flow chamber was developed, which allows to examine adhesion forces of complete biofilms, whereby samples of overgrown surfaces can be variably integrated into the flow chamber. By combination with optical coherence tomography (OCT) adhesion under increasing shear stress can be observed. For evaluation of present flow regimes, the complementation with computational fluid dynamics (CFD) simulation was realized. To demonstrate the comparability with existing systems, feasible comparable measurements with a rotational rheometer were conducted. Experiments were conducted exemplarily with two different cyanobacterial biofilms, however, this method should be applicable to any type of biofilm.

2 | MATERIALS AND METHODS

2.1 | Strains and precultures

In this study the terrestrial cyanobacteria *Trichocoleus desertorum* and *Nostoc* sp. (strain number SAG 26.92) were used, which were kindly provided by Prof. Dr. Burkhard Büdel (Department of Plant Ecology and Systematics; RPTU Kaiserslautern-Landau). Both strains originate from desert soil, *T. desertorum* from Namibia and *Nostoc* sp. from Nizzana in Israel. As precultures 300 mL shaking flasks without baffles with 50 mL of standard BG11 medium (Stanier et al., 1979) were inoculated with

0.1 g cell wet weight. Precultures were incubated in a shaking incubator (Multitron S-000115689; Infors HT) at 120 rpm (2.5 cm eccentricity), at a temperature of 30°C and continuous illumination with 100 $\mu mol_{photons}$ m^{-2} s^{-1}. Light intensity was controlled with a quantum sensor (radiometer LI-1400 with Licor 190A; LI-COR-Biosciences). For transfer of the cells into biofilm cultivation systems, cells were harvested by centrifugation for 15 min at 8000g.

2.2 | Characterization of surface substrates

For characterization of utilized surface materials roughness and hydrophobicity were analyzed. Roughness was determined via atomic force microscopy (JPK NanoWizard 3 System; JPK Instruments AG). Hydrophobicity was examined by measurement of the contact angle with an optical contact angle measuring system (OCA 15plus; DataPhysics Instruments GmbH) and data analysis with the software SCA 20 (DataPhysics Instuments GmbH).

2.3 | Development of the flow chamber

To easily analyse biofilms for existing adhesion forces after cultivation, a special flow chamber was developed (see Figure 1). The flow chamber consists of a 145 mm long borosilicate glass tube with an inner diameter of 45 mm. Threads at both ends can be used to provide the tube with GL25 lids into which glass tubes for the inlet (inner diameter 9 mm) and outlet (inner diameter 7 mm) of a liquid flow are inserted. A cultivation surface (75 x 20 x 2 mm) covered with biofilm can be placed in the flow chamber, which is fixed in the glass tube by two side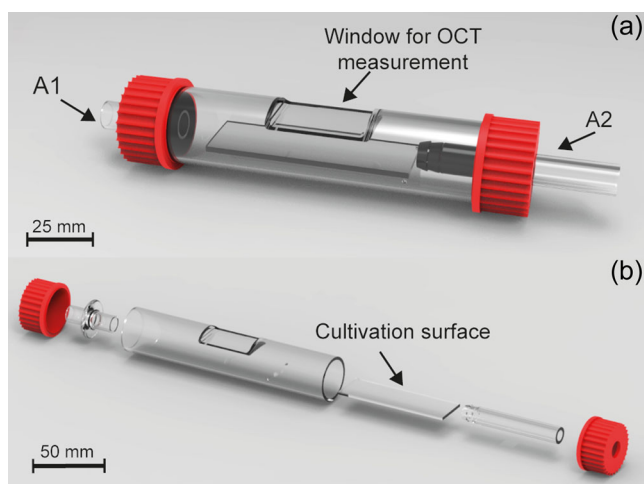 punctures. Liquid can flow over the biofilm via the two connections and by adjusting the flow speed until the biofilm detaches, adhesion forces can be examined. To be able to continuously document the influence on the biofilm, there is a planar viewing window with a 5 mm lowering in the chamber, which allows recording by OCT and prevents signal distortion due to possible light refraction at the glass curve.

2.4 | Simulation of flow regimes and shear rate

To evaluate the flow in the flow chamber and its influence on the biofilm, CFD simulations were performed with a varying flow velocity. Therefore, the CFD software COMSOL Multiphysics (COMSOL Inc.) was used with the k-ω-shear stress transport (SST) model (Menter, 1992). The k-ω-SST model calculates the turbulence of a flow via turbulent kinetic energy k and turbulent dissipation rate ω. The model uses two differential equations, for the solution of which boundary conditions for k and ω are necessary. These can be estimated for the entry into the flow chamber via the turbulent intensity I (Equation 1).

$$I = \frac{v'}{v_{mean}} = 0,16 \times Re^{-\frac{1}{8}} \quad (1)$$

It indicates the ratio of the fluctuation speed v' to the mean flow speed v_{mean} and thus describes the turbulence introduced into the system. To calculate k_{In} and ω_{In}, kinetic energy and turbulent dissipation rate at the entrance of the flow chamber, Equation 2 and Equation 3 are used.

$$k_{In} = \frac{3}{2} \times (v_{mean} \times I) \quad (2)$$

$$\omega_{In} = C_\mu^{\frac{1}{4}} \times k_{In}^{\frac{1}{2}} \times l_T^{-1} \quad (3)$$

Hereby, C_μ is a model parameter and l_T is the turbulent length, which describes the size of the largest turbulences. Additionally, the k-ω-SST model includes a term for SST. This allows the usage of the model to describe turbulence in the free stream as well as close to the wall. As a framework for all simulations, the inside diameter of the inlet pipe (9 mm) was set as the characteristic length (L). To calculate the superficial velocity, the volume flow used was related to the cross-section of the inlet pipe. To simulate flow processes in the flow chamber the superficial velocities were chosen as frame conditions, which led to biofilm detachment from the surface in the experiments shown later. Thereby, the conditions at the entrance to the flow chamber (diameter 9 mm) at respective velocities are given (see Table 1), which were used to determine occurring shear forces. The dynamic viscosity of water at 20°C η = 0.001 Pa s was assumed for the overflowing liquid, which is comparable for mineral salt media. In combination with experimental results the simulation data can be used to describe the shear forces necessary for detachment of a biofilm from a substrate and thus evaluate adhesion strength.

FIGURE 1 CAD model of the flow chamber for the investigation of biofilm adhesion. (a) Assembled flow chamber. (b) Exploded view of the flow chamber. A1: Connection for supplying medium. A2: Connection for the discharge of medium. The CAD model was generated with Solid Edge ST9 (Siemens PLM Software). OCT, optical coherence tomography.

TABLE 1 Overview of the superficial velocity in the flow chamber examined in the simulation as well as the associated boundary conditions.

v_s [m s^{-1}]	Re [−]	I [−]	k_{In} [m^2 s^{-2}]	ω_{In} [s^{-1}]
0.017	150	0.086	3.05×10^{-6}	1.52[a]
0.026	237	0.081	6.81×10^{-6}	2.27[a]
0.040	356	0.077	1.38×10^{-5}	3.23[a]
0.053	475	0.074	2.29×10^{-5}	4.16[a]
0.078	706	0.070	4.58×10^{-5}	5.89
0.105	943	0.068	7.61×10^{-5}	7.59
0.131	1181	0.066	1.12×10^{-4}	9.23
0.158	1418	0.065	1.55×10^{-4}	10.84
0.236	2127	0.061	3.16×10^{-4}	15.45
0.289	2598	0.060	4.48×10^{-4}	18.41
0.420	3784	0.057	8.66×10^{-4}	25.58

Note: The conditions at the entrance to the flow chamber (Ø 9 mm) are given.

Abbreviations: I, turbulent intensity; kIn, turbulent kinetic energy; Re, Reynolds number; vs, superficial velocity; ωIn, turbulent dissipation rate.
[a]Here a completely laminar model was used for the calculation since no mixing occurred.

2.5 | Examination of flow regimes in the flow chamber

To examine the flow profile in the flow chamber, liquid was pumped through the chamber at different speeds (Pumpdrive 5206; Heidolph). To make the flow visible, a rhodamine B solution with a concentration of 1 mg mL^{-1} was injected with a cannula into the silicone tube 5 cm before entering the flow chamber. At the same time, video recordings were made with an EOS 650D camera (Canon). The recordings were then assessed for discernible turbulence in the rhodamine-colored flow.

2.6 | Experimental procedure in the flow chamber

To investigate surface adhesion of emerse cultured biofilms from *T. desertorum* and *Nostoc* sp., 75 × 20 × 2 mm plates made of borosilicate glass or polymethylmethacrylat (PMMA) were inoculated on an area of 20 × 10 mm with 100−200 mg of wet biomass. Surfaces were sandblasted (borosilicate glass) or scratched with abrasive paper (PMMA, grain size 120) for better primary adhesion of the biomass. Inoculated surfaces were placed in a transparent cultivation unit (length: 22.5 cm, width: 5.8 mm, height: 6.3 mm) (see Figure 2a).

For generation of aerosol, liquid BG11 medium was pumped in a vessel with an ultrasonic transducer (NW-80E-01; TDK Europe), which was already described by Strieth et al. (2017) and is based on a patent by Schmidt and Just (WO2007068467A1, 2006). The transducer vessel used here, had one additional connection over the ultrasonic
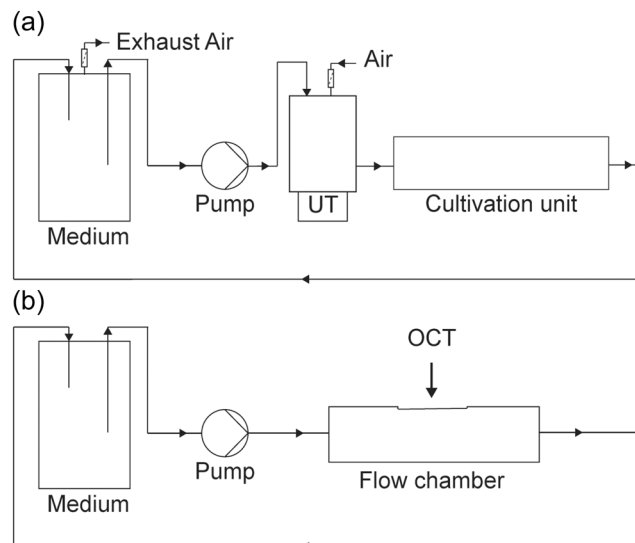

FIGURE 2 (a) Setup for cultivation of cyanobacterial biofilms on surfaces. (b) Setup for examination of surface adhesion of cyanobacterial biofilms in the flow chamber. OCT, optical coherence tomography; UT, ultrasonic transducer.

transducer, to ensure a constant medium level over the transducer. From the transducer vessel aerosol was transferred into the cultivation unity by application of 1 L min^{-1} compressed air. Condensed medium and waste aerosol were recycled from the cultivation unit back into the medium supply vessel. Cultivations were conducted at 24°C, continuous aerosol supply and illumination at an intensity of 100 μmol$_{photons}$ m^{-2} s^{-1} with a light/dark rhythm of 14 h/10 h.

After 0, 1, 2, 3, 4, 7, and 14 days, 3−5 replicates were removed to examine the surface adhesion in the flow chamber. Therefore, one overgrown surface was placed in the flow chamber, which was filled with medium and connected to a pump (Pumpdrive 5206; Heidolph) (see Figure 2b). The flow chamber was positioned under the OCT (OCT G_900; Thorlabs), to be able to make video recordings through the viewing window of the chamber. The used OCT allowed documentation of biofilm length of 15 mm starting from the inlet side of the flow chamber. Subsequently, the pump speed was increased stepwise until the biofilm completely detached from the surface. This process was repeated for all biofilm replicates. Additionally, OCT data were used to calculate the standardized biofilm roughness Ra* as described by Murga et al. (1995).

2.7 | Experimental procedure with the rotational rheometer

To investigate the surface adhesion of biofilms using a rotational rheometer, surfaces made of borosilicate glass were inoculated with biomass and cultivated analogously to experiments in the flow chamber. The only difference was the shape of the surfaces: To be able to attach the surfaces later in the rheometer, round surfaces with a diameter of 50 mm were used. A round surface area with a diameter of

20 mm was inoculated onto these. After 0, 2, 4, 7, and 14 days, 3–4 replicates were examined with a Kinexus ultra+ rotational rheometer (Netzsch–Gerätebau GmbH). Biofilm-covered surfaces were placed under a 20 mm plate on the optical cell measuring geometry and covered with BG11 medium. Sealing rings were used to keep the liquid in the measuring gap. The upper plate was then approximated to such an extent that the lower edge of the plate was wetted with liquid. This procedure was chosen instead of a fixed gap between biofilm and plate, since a fixed gap was not possible due to the roughness of biofilm surface and included air bubbles. Therefore, a full contact of upper plate geometry and biofilm was not possible without destroying the biofilm structure itself. Accordingly, it was chosen to let biofilm and upper plate not directly contact with each other, and so, no direct forces of the rheometer were applied on the biofilm but were indirectly transferred by the liquid between biofilm and rheometer plate.

The shear rate required to detach the biofilm was determined by logarithmic increasing of the shear rate from 1 to $1000\,s^{-1}$ with 10 steps per decade using a step function. The biofilm detachment event was documented by video recordings from below the surface through an optical measuring cell. The optical measuring cell is part of the rotational rheometer and consists of a stainless steel cylinder with a glass plate on which the biofilm covered surface was placed. On top of this surface, an O-ring seal separated the glass surface from the union nut. An endoscope camera was placed in the stainless steel cylinder to observe the detachment of the biofilm from below. Additionally, a solvent trap was installed above the union nut to prevent the BG11 medium from evaporating during the measurement.

A schematic is supplied by the manufacturer's [LINK NETZSCH], with the difference that a UV cell is shown there. The setup of the cell is similar to the optical measuring cell, but the UV accessory has to be replaced by an LED light source and the UV source by the endoscope camera

2.8 | EPS extraction

After detachment of the biofilm from the surface the biomass was collected and EPS were extracted by a combined method with heat and ultrasonication, which was already described (Strieth et al., 2020). After extraction, EPS and remaining biomass were lyophilized (LOC-1M Alpha 2-4; Christ) at −20°C and 1 mbar for 24 h. The EPS content in relation to total cell dry weight (CDW; remaining biomass + extracted EPS) was calculated.

2.9 | Quantification of rhamnolipids in the EPS

A photometric assay according to Chandrasekaran and Bemiller was carried out to determine the rhamnolipid content in the EPS (Chandrasekaran & Bemiller, 1980). The protocol was performed according to Schlegel (2015). Freeze-dried EPS samples were resuspended in 300 µL deionized water for sample preparation. For calibration, rhamnolipid standards in the concentrations 2.5, 12.5, 25,

37.5, and $50\,mg\,L^{-1}$ in 300 µL deionized water were measured. Samples and standards were treated equally for further sample preparation. For extraction of rhamnolipids, 600 µL of ethyl acetate were added to each sample and shaken in the vibrating ball mill for 10 min at a shaking frequency of $30\,s^{-1}$. The supernatant was then separated and removed by centrifugation at 8600g for 1 min. Another 600 µL of ethyl acetate were added to the remaining pellet and the further extraction steps were repeated. Ethyl acetate supernatants were combined and evaporated at 90°C over 30–60 min. After adding 100 µL deionized water, 100 µL orcinol solution (1.6% w/v) and 800 µL 60% (v/v) sulfuric acid, samples were incubated at 80°C for 30 min and then 10 min at room temperature. Two hundred microliters of standards or samples were pipetted into 96-well plates. Absorbance measurements were carried out at 405 nm in a multilabel plate reader type Victor X4 (PerkinElmer).

3 | RESULTS AND DISCUSSION

3.1 | Experimental determination of flow regimes in the flow chamber

To experimentally investigate the flow velocity at which the different flow regimes occur in the flow chamber, the pink dye rhodamine was injected into the flow chamber at various pump speeds. The visualized flow profile was recorded with a camera. Up to a superficial velocity of $0.026\,m\,s^{-1}$, a completely laminar flow was discernible (Table 2 and Supporting Information: Figure 1). The first visible macro mixing occurred at a speed of $0.040\,m\,s^{-1}$. Starting at $0.078\,m\,s^{-1}$ first backmixings were observed in the flow chamber. At a flow speed of $0.289\,m\,s^{-1}$ and a Reynolds number of 2598 (see Table 1) the transition into turbulent flow was reached. Observed mixing at low Reynolds numbers might be caused by constructional differences to an ideal plug flow reactor, such as the changing cross section after entry into the chamber or the cultivation surface, which is placed in the chamber.

3.2 | Characterization of cultivation surfaces

The cultivation surfaces examined in the flow chamber and with rheometry were analyzed concerning surface roughness and hydrophobicity. Hereby, medium on PMMA showed with 73.0 ± 1.7°a

TABLE 2 Flow regimes in the flow chamber with increasing superficial velocity.

Flow regime	Superficial velocity v_s [m s^{-1}]	Reynolds number Re [−]
Laminar	0.000–0.236	0–2127
Transitional/turbulent	0.289–0.420	2598–3784

Note: The flow profile was visualized using rhodamine injections. The superficial velocity vs for entry into the flow chamber is indicated.

—WILEY—

higher contact angle as on borosilicate glass (69.9 ± 4.1°). With an angle <90° both substrates are hydrophilic (Law, 2014), which simplifies adhesion of organisms with hydrophilic surface. The glass surface used for examination in the flow chamber showed with a root-mean-squared roughness R_q of 209.5 ± 53.6 nm compared to 73.0 ± 1.7 nm a higher surface roughness than PMMA. However, between glass plates used in the flow chamber and glass discs (R_q = 204.4 ± 77.3 nm) in the rotational rheometer no differences could be determined. Thus, differences in surface adhesion can be solely traced back to the measurement methods, which allows the comparison of results from the flow chamber and the rotational rheometer.

3.3 | Examination of biofilm adhesion in the flow chamber

Biofilms of *T. desertorum* and *Nostoc* sp. with varied cultivation time were analyzed in the flow chamber concerning surface adhesion. In all the experiments carried out no detachment of individual fragments from the biofilm could be recorded, but the biofilm always detached in one piece (exemplary pictures in Supporting Information: Figure 2). Hence, the cohesion between the cells is presumably stronger than the adhesion to the surface. Investigation of partial

detachment of biofilms is as well possible using the flow chamber, however, in this case a more comprehensive assessment of adhesion would be required, as unlike complete detachment of the biofilm, no simple yes/no answer can be given to adhesion at a given flow rate. Both strains showed increased adhesion to borosilicate glass compared to the adherence to PMMA (see Figure 3a,c). Improved adhesion to glass can be attributed to increased surface roughness and the slightly more hydrophilic surface. Biofilms from *Nostoc* sp. on PMMA already detached when the flow chamber was filled with liquid, which is why no data is shown. During previous cultivation in aerosol, however, there was no detachment of biofilms, which can be attributed to the lower shear stress in this system. Over the cultivation period, a continuous increase in the flow rate necessary for detachment and thus the strength of the adhesion was determined for *T. desertorum* on both surface materials and for *Nostoc* sp. on borosilicate glass. The decrease in adhesion of *T. desertorum* to glass towards the end of the cultivation could indicate the growth phase of the biofilm at this time of cultivation (Figure 3). Biofilms may already have been in the stationary phase after 14 days, after which parts of the biofilm also begin to detach to colonize new surfaces. For example, Sandal et al. observed detachment of biofilms of *Histophilus somnus* after only 7 days of cultivation (Sandal et al., 2007). Overall, biofilms of *T. desertorum* only detached at higher flow rates compared to *Nostoc* sp.
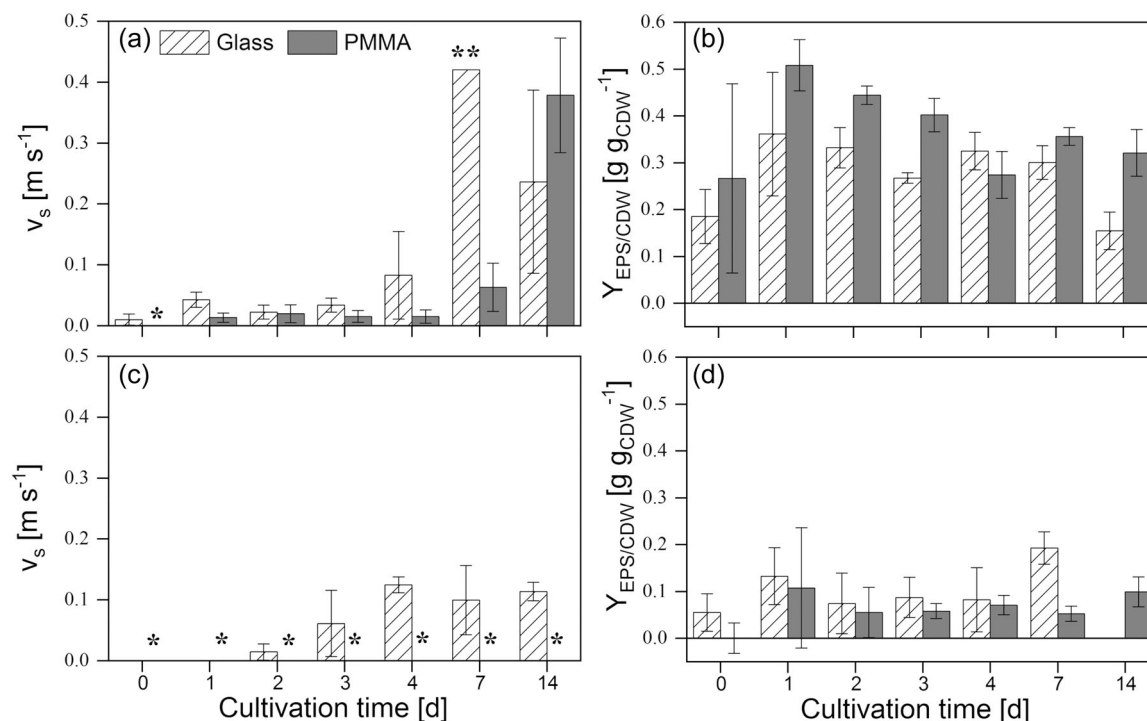

FIGURE 3 Surface adhesion of (a) *Trichocoleus desertorum* and (c) *Nostoc* sp. on borosilicate glass and PMMA over a cultivation time of 14 days. Corresponding EPS contents in relation to cell dry weight (CDW) are given for (b) *T. desertorum* and (d) *Nostoc* sp. *No values are given, since the biofilm detached already when setting the flow chamber up. **The maximum pump speed was reached and was not sufficient to detach the biofilm. Mean values and standard deviations from 3 to 5 replicates are given. EPS, extracellular polymeric substances; PMMA, polymethylmethacrylat.

3.3.1 | Connection between adhesion, EPS content, and biofilm roughness

The higher surface adhesion of *T. desertorum* could be attributed to increased EPS contents in *T. desertorum* compared to *Nostoc* sp. (Figure 3b,d). In addition, an increase in EPS content was observed for both strains on both materials at the beginning of cultivation, which gradually decreased again in the further course of cultivation. This can in turn be explained by the different development phases of biofilms. In the first stages of the biofilm, EPS is increasingly formed to enable cells to adhere more strongly to the surface, which Carniello et al. (2018) and Tolker-Nielsen et al. (2015) described in detail. There is also the possibility that, when biomass is transferred to a new system, EPS is first increasingly used to store nutrients, which are afterwards metabolized (Flemming, 2011; Li et al., 2016). However, since not only the amount of EPS but above all their composition is crucial for adhesion, an analysis of the EPS components would be necessary for a more precise assessment. For example, an influence of rhamnolipids as a component of EPS has already been described (Davey et al., 2003). Another influencing factor that can explain the differences between the strains is the surface roughness of biofilms themselves. Therefore, the standardized biofilm roughness Ra* was determined from the OCT images of the biofilms. *T. desertorum* with values between 0.18 ± 0.02 and 0.23 ± 0.13 showed a reduced roughness R_a^* compared to the biofilms of *Nostoc* sp. with a roughness of 0.24 ± 0.05 to 0.35 ± 0.08 (Table 3). Here, it is conceivable that due to greater roughness, *Nostoc* sp. offered a larger contact surface for overflowing liquid and the biofilm therefore detached from the surface even at lower flow velocities. To investigate this possibility in more detail, an additional introduction of biofilm surface structure into the flow simulation would be of interest.

3.3.2 | Calculation of shear rate and shear strength using CFD

Superficial velocities required for detachment of biofilms were used to calculate shear rate γ_W prevailing at the detachment event and shear strength τ_W of the biofilm using the CFD simulation described before (see Table 3). For *T. desertorum* on borosilicate glass and PMMA as well as for *Nostoc* sp. on borosilicate glass, there is a continuous increase in adhesion over the cultivation period. However, only a slight increase is noted in the first days of cultivation, after which the adhesion suddenly increases significantly in a few days. This suggests that after inoculating the surfaces with wet biomass from a suspension preculture, there is an initial adaptation phase to the surface-associated growth in the aerosol environment. For *T. desertorum* on glass, a flow at a speed of $0.083 \pm 0.072 \text{ m s}^{-1}$ is necessary to detach the biofilm on day 4 of cultivation, which continues to increase until Day 7 ($v_s > 0.420 \text{ m s}^{-1}$). *Nostoc* sp. as well showed an increased adhesion after 4 days ($v_s = 0.125 \pm 0.013 \text{ m s}^{-1}$), with only minor changes occurring in the following days. On PMMA, the adaptation phase for *T. desertorum*

was longer than on glass and only ended between 7 and 14 days. No meaningful values could be determined for *Nostoc* sp. on PMMA, since biomass detached from the surface before starting the flow in the flow chamber. For *T. desertorum* on borosilicate glass a maximum strength τ_W of over 0.25 Pa was achieved, on PMMA of 0.23 ± 0.04 Pa and for *Nostoc* sp. of 0.069 ± 0.01 Pa on borosilicate glass. These values are in the range of the shear strengths described in literature for biofilms of other microorganisms. Lopez-Mila et al. (2018) detected an almost complete removal of *E. coli* on N-(2-hydroxypropyl)methacrylamide at a value of about 0.025 Pa. Hassan et al. (2012) examined adhesion of the cyanobacterium *Oscillatoria* sp. on steel surfaces with varied roughness, where almost 70% of biomass detached from the surface at 0.044 Pa. The highest values with up to 50 Pa after 32 days of cultivation are described by Ohashi and Harada (1994) for an unspecified biofilm of denitrifying bacteria, whereby also an increase in adhesion over the cultivation period was determined. Differences in the shear strengths between the results achieved in this work and given literature references can be traced back to strain-specific adhesion, type and duration of cultivation, surface material used, and applied test methods. In summary, surface adhesion of biofilms was successfully determined in the flow chamber in combination with CFD simulation, stating the shear strength. An increase in surface adhesion with increasing biofilm age was found, as well as a connection with the EPS content of the biofilm. The results obtained match the phases of biofilm development and adhesion forces described for other biofilms. In addition, strain-specific differences and an influence of surface material could be determined. Instead of combining the flow chamber with OCT, it is also convenient to document biofilm detachment with a camera, making the flow chamber a cost-effective and easy-to-implement method. To investigate, whether results from the flow chamber developed in-house are comparable to results achieved with other methods, the following chapter describes adhesion experiments using a rotational rheometer and compares them with results obtained with the flow chamber.

3.4 | Examination of biofilm adhesion using rheometry

To test the comparability of results obtained in the self-developed flow chamber with other methods, adhesion of biofilms of *T. desertorum* and *Nostoc* sp. on glass was examined using a rotational rheometer. Rotational rheometry is an established method for analysis of material properties, however, experiments are time consuming and the equipment is costly. Furthermore, shear stress is generated by rotation, which differs from conditions in most cultivation systems and thus influences comparability. Therefore, experiments with the flow chamber as an easy to implement and cheap alternative were compared with results from a rotational rheometer. Analogous to tests in the flow chamber, the shear rate required to remove biofilms and, consequently, the surface adhesion increased with biofilm age (see Figure 4). In addition, *T. desertorum*

TABLE 3 Experimental results from the flow chamber in combination with the simulation with the k-ω-SST model in COMSOL multiphysics.

Cultivation time [d]	0	1	2	3	4	7	14
Trichocoleus desertorum on borosilicate glass							
Superficial velocity v_s [m s^{-1}]	0.010 ± 0.009	0.043 ± 0.013	0.022 ± 0.011	0.034 ± 0.011	0.083 ± 0.072	>0.420[a]	0.236 ± 0.150
Reynolds number Re	90 ± 82	386 ± 114	201 ± 103	305 ± 103	747 ± 647	>3784[a]	2127 ± 1353
Shear rate γ_W [s^{-1}]	1.64 ± 1.50	13.32 ± 5.65	4.97 ± 4.46	9.42 ± 4.46	44.72 ± 47.47	>251.25[a]	144.74 ± 98.47
Shear strength τ_W [Pa]	1.6 ± 1.5 × 10^{-3}	1.3 ± 0.6 × 10^{-2}	5.0 ± 4.5 × 10^{-3}	9.4 ± 4.5 × 10^{-3}	4.5 ± 4.7 × 10^{-2}	>2.5 × 10^{-1}[a]	1.4 ± 1.0 × 10^{-1}
EPS content [g g$_{CDW}^{-1}$]	0.19 ± 0.06	0.36 ± 0.13	0.33 ± 0.04	0.27 ± 0.01	0.32 ± 0.04	0.30 ± 0.04	0.15 ± 0.04
Biofilm thickness [µm]	1119 ± 476	740 ± 70	861 ± 178	931 ± 282	1173 ± 299	920 ± 170	1042 ± 97
Roughness R$_a$*	0.16 ± 0.01	0.14 ± 0.03	0.21 ± 0.06	0.16 ± 0.02	0.21 ± 0.05	0.20 ± 0.05	0.18 ± 0.05
T. desertorum on PMMA							
Superficial velocity v_s [m s^{-1}]	0.00 ± 0.00	0.013 ± 0.007	0.020 ± 0.015	0.015 ± 0.010	0.015 ± 0.011	0.063 ± 0.040	0.378 ± 0.094
Reynolds number Re	0 ± 0	120 ± 67	179 ± 131	137 ± 86	134 ± 99	566 ± 357	3405 ± 849
Shear rate γ_W [s^{-1}]	0.00 ± 0.00	2.19 ± 1.22	4.63 ± 4.47	2.85 ± 2.14	2.88 ± 2.47	27.38 ± 19.80	233.74 ± 39.15
Shear strength τ_W [Pa]	0.0 ± 0.0	2.2 ± 1.2 × 10^{-3}	4.6 ± 4.5 × 10^{-3}	2.9 ± 2.1 × 10^{-3}	2.9 ± 2.5 × 10^{-3}	2.7 ± 2.0 × 10^{-2}	2.3 ± 0.4 × 10^{-1}
EPS content [g g$_{CDW}^{-1}$]	0.27 ± 0.20	0.51 ± 0.05	0.44 ± 0.02	0.40 ± 0.04	0.27 ± 0.05	0.36 ± 0.02	0.32 ± 0.05
Biofilm thickness [µm]	n. d.	1528 ± 76	1647 ± 105	1552 ± 195	1582 ± 289	1305 ± 119	1214 ± 72
Roughness R$_a$*	n. d.	0.13 ± 0.03	0.08 ± 0.02	0.18 ± 0.02	0.12 ± 0.04	0.18 ± 0.03	0.23 ± 0.13
Nostoc sp. on borosilicate glass							
Superficial velocity v_s [m s^{-1}]	0.00 ± 0.00	0.00 ± 0.00	0.014 ± 0.013	0.061 ± 0.055	0.125 ± 0.013	0.100 ± 0.57	0.114 ± 0.015
Reynolds number Re	0 ± 0	0 ± 0	129 ± 120	550 ± 491	1121 ± 119	898 ± 511	1023 ± 137
Shear rate γ_W [s^{-1}]	0.00 ± 0.00	0.00 ± 0.00	2.93 ± 3.03	28.71 ± 26.83	68.72 ± 10.38	53.57 ± 39.32	60.07 ± 11.98
Shear strength τ_W [Pa]	0.0 ± 0.0	0.0 ± 0.0	2.9 ± 3.0 × 10^{-3}	2.9 ± 2.7 × 10^{-2}	6.9 ± 1.0 × 10^{-2}	5.4 ± 3.9 × 10^{-2}	6.0 ± 1.2 × 10^{-2}
EPS content [g g$_{CDW}^{-1}$]	0.05 ± 0.04	0.13 ± 0.06	0.07 ± 0.06	0.09 ± 0.04	0.08 ± 0.07	0.19 ± 0.03	n. d.
Biofilm thickness [µm]	462 ± 35	391 ± 40	475 ± 30	422 ± 10	889 ± 217	1004 ± 185	1117 ± 99
Roughness R$_a$*	0.27 ± 0.15	0.34 ± 0.03	0.24 ± 0.05	0.35 ± 0.08	0.26 ± 0.08	0.27 ± 0.05	0.28 ± 0.08

Note: *Nostoc* sp. on PMMA: Since *Nostoc* sp. had no measurable adhesion to PMMA, no values could be calculated.

Abbreviations: CDW, cell dry weight; EPS, extracellular polymeric substances; n. d., not detectable; PMMA, polymethylmethacrylat; SST, shear stress transport.

[a]The maximum pump speed was reached.

again showed an increased surface adhesion compared to *Nostoc* sp. in combination with a higher EPS content. An adaptation phase at the beginning of the cultivation was as well determined with rheometer measurements: for *T. desertorum* only after 4 days and for *Nostoc* sp. only after 7 days a clear increase was detected. For *T. desertorum*, stronger adhesion goes hand in hand with an increasing EPS content in the first days of cultivation, which again may be related to the phases of biofilm formation and subsequent increase of surface adhesion (Garrett et al., 2008).

Compared to the results from the flow chamber (see Table 3), the shear rate required to remove the biofilm using a rotational rheometer was higher. For *T. desertorum*, shear rates of up to 772.1 ± 131.5 s^{-1} were measured in the rheometer and a maximum of 251.25 s^{-1} was reached in the flow chamber (corresponds to the highest possible pumping speed of the used pump). For *Nostoc* sp. the highest shear rate in the rheometer was 185.9 ± 190.6 s^{-1}, in the flow chamber it was 68.72 ± 10.38 s^{-1}. This difference could be attributed to the different form of shear stress application: In the flow chamber, the biofilm is overflown horizontally, whereas in the rheometer a rotational movement is applied. However, the results are in the same order of magnitude and show the same tendencies with regard to the different strength of adhesion of the two strains as well as the increase in adhesion strength in the course of cultivation. Therefore, the same conclusions can be drawn via both methods.
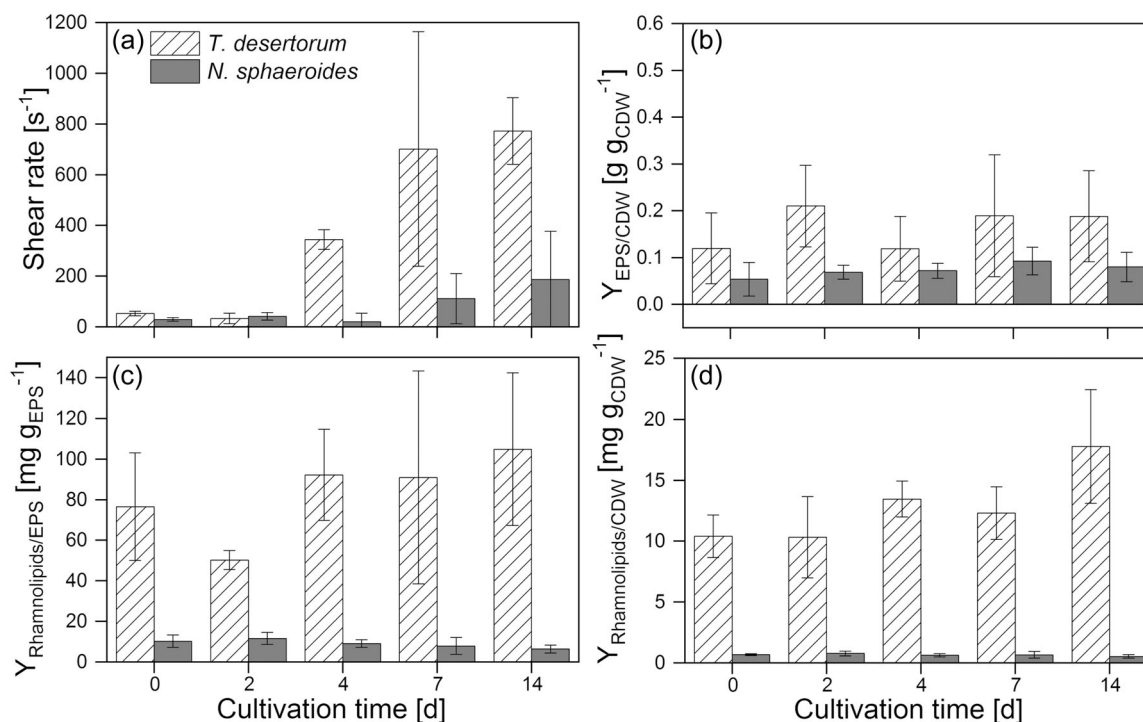
FIGURE 4 Surface adhesion of (a) *Trichocoleus desertorum* and *Nostoc* sp. on borosilicate glass over a cultivation time of 14 days. Measurements were conducted with a rotational rheometer. (b) Corresponding EPS contents in relation to cell dry weight (CDW). Rhamnolipid content in EPS (c) and in relation to total CDW (d). Mean values and standard deviations from 3 to 5 replicates are given. EPS, extracellular polymeric substances.

Since an influence of rhamnolipids in EPS on biofilm formation and adhesion has been described before, the rhamnolipid content in EPS of biofilms examined by rheometry was determined (see Figure 4c,d). In literature so far mainly biofilms of *Pseudomonas aeruginosa* have been analyzed with regard to their rhamnolipid production, since they are of industrial interest (Chong & Li, 2017). Concerning surface adhesion, Wigneswaran et al. (2016) achieved an increased biofilm formation for a rhamnolipid-producing *Pseudomonas putida* strain compared to a control strain. Nickzad and Déziel (2014) and Chrzanowski et al. (2012) summarize various studies on the influence of rhamnolipids on biofilm formation, however, this has not been described for cyanobacteria so far. In fully developed biofilms, rhamnolipids also play an important role in maintaining the complex biofilm architecture, such as the formation of channels in the biofilm (Davey et al., 2003). For *T. desertorum* the rhamnolipid content increased from 10.4 ± 1.8 to $17.78 \pm 4.7\,\mathrm{mg\,g_{CDW}}^{-1}$ over the cultivation period (see Figure 4d). In comparison, the values for *Nostoc* sp. are lower with $0.69 \pm 0.08\,\mathrm{mg\,g_{CDW}}^{-1}$ at the beginning of cultivation and $0.53 \pm 0.15\,\mathrm{mg\,g_{CDW}}^{-1}$ after 14 days, with an almost constant rhamnolipid content over the cultivation period. The increased rhamnolipid content in *T. desertorum* may thus be in conjunction with the stronger surface adhesion compared to *Nostoc* sp.

In summary, the values obtained in the experiments with the flow chamber and with the rotational rheometer are of the same order of magnitude and show comparable tendencies. Both methods show the same differences between cyanobacterial strains and the same trends regarding adhesion during biofilm cultivation. Consequently, these results demonstrate that the developed flow chamber is an easy-to-implement, cost-effective method for the rapid investigation of surface adhesion of biofilms.

4 | CONCLUSIONS

In this work with the flow chamber a simple method for examination of biofilm adhesion on variable surfaces was presented. Results obtained with the flow chamber were comparable to examinations with a rotational rheometer. Hereby, with both methods an increase of biofilm adhesion with increasing biofilm age was detected, with stronger adhesion of the strain *T. desertorum* compared to *Nostoc* sp. With the flow chamber additionally a stronger adhesion on borosilicate glass than on PMMA was observed. Therefore, the flow chamber enables fast preliminary investigations to select a suitable combination of production organism and cultivation surface in advance of larger production processes.

AUTHOR CONTRIBUTIONS

Judith Stiefelmaier: Conceptualization, analysis and interpretation of the data, writing—original draft. **Dorina Strieth**: Conceptualization, analysis and interpretation of the data, writing—review and editing. **Susanne Schaefer**: Investigation, data curation, analysis of the data,

CONFLICT OF INTEREST STATEMENT

The authors declare no conflict of interest.

DATA AVAILABILITY STATEMENT

The data that support the findings of this study are available from the corresponding author upon reasonable request.

ORCID

Judith Stiefelmaier http://orcid.org/0000-0002-5628-1927
Roland Ulber http://orcid.org/0000-0002-7674-0967

REFERENCES

Blanken, W., Janssen, M., Cuaresma, M., Libor, Z., Bhaiji, T., & Wijffels, R. H. (2014). Biofilm growth of *Chlorella sorokiniana* in a rotating biological contactor based photobioreactor. *Biotechnology and Bioengineering*, 111(12), 2436–2445. https://doi.org/10.1002/bit.25301

Bryers, J. D., & Ratner, B. D. (2004). Bioinspired implant materials befuddle bacteria. *ASM News*, 70(5), 232–237.

Carniello, V., Peterson, B. W., van der Mei, H. C., & Busscher, H. J. (2018). Physico-chemistry from initial bacterial adhesion to surface-programmed biofilm growth. *Advances in Colloid and Interface Science*, 261, 1–14. https://doi.org/10.1016/j.cis.2018.10.005

Castillejo, N., Martínez-Hernández, G. B., Goffi, V., Gómez, P. A., Aguayo, E., Artés, F., & Artés-Hernández, F. (2018). Natural vitamin B12 and fucose supplementation of green smoothies with edible algae and related quality changes during their shelf life. *Journal of the Science of Food and Agriculture*, 98(6), 2411–2421. https://doi.org/10.1002/jsfa.8733

Chandrasekaran, E. V., & Bemiller, J. N. (1980). Constituent analyses of glycosaminoglycans. *Methods in Carbohydrate Chemistry*, 8, 95–96.

Chong, H., & Li, Q. (2017). Microbial production of rhamnolipids: Opportunities, challenges and strategies. *Microbial Cell Factories*, 16(1), 137. https://doi.org/10.1186/s12934-017-0753-2

Chrzanowski, Ł., Ławniczak, Ł., & Czaczyk, K. (2012). Why do microorganisms produce rhamnolipids. *World Journal of Microbiology & Biotechnology*, 28(2), 401–419. https://doi.org/10.1007/s11274-011-0854-8

Davey, M. E., Caiazza, N. C., & O'Toole, G. A. (2003). Rhamnolipid surfactant production affects biofilm architecture in *Pseudomonas aeruginosa* PAO1. *Journal of Bacteriology*, 185(3), 1027–1036. https://doi.org/10.1128/jb.185.3.1027-1036.2003

Davoudi, N., Huttenlochner, K., Chodorski, J., Schlegel, C., Bohley, M., Müller-Renno, C., Aurich, J. C., Ulber, R., & Ziegler, C. (2017). Adhesion forces of the sea-water bacterium *Paracoccus seriniphilus* on titanium: Influence of microstructures and environmental conditions. *Biointerphases*, 12(5), 05G606. https://doi.org/10.1116/1.5002676

Fleming, E. D., & Castenholz, R. W. (2007). Effects of periodic desiccation on the synthesis of the UV-screening compound, scytonemin, in Cyanobacteria. *Environmental Microbiology*, 9(6), 1448–1455. https://doi.org/10.1111/j.1462-2920.2007.01261.x

Flemming, H. C. (2011). The perfect slime. *Colloids and Surfaces B: Biointerfaces*, 86(2), 251–259. https://doi.org/10.1016/j.colsurfb.2011.04.025

Flemming, H. C., & Wingender, J. (2010). The biofilm matrix. *Nature Reviews Microbiology*, 8(9), 623–633. https://doi.org/10.1038/nrmicro2415

Garcia-Pichel, F., Belnap, J., Neuer, S., & Schanz, F. (2003). Estimates of global cyanobacterial biomass and its distribution. *Algological Studies*, 109(1), 213–227. https://doi.org/10.1127/1864-1318/2003/0109-0213

Garrett, T. R., Bhakoo, M., & Zhang, Z. (2008). Bacterial adhesion and biofilms on surfaces. *Progress in Natural Science*, 18(9), 1049–1056. https://doi.org/10.1016/j.pnsc.2008.04.001

Hassan, M. F., Lee, H. P., & Lim, S. P. (2012). Effects of shear and surface roughness on reducing the attachment of *Oscillatoria* sp. filaments on substrates. *Water Environment Research*, 84(9), 744–752. https://doi.org/10.1002/j.1554-7531.2012.tb00283.x

Hedges, S. B., Chen, H., Kumar, S., Wang, D. Y. C., Thompson, A. S., & Watanabe, H. (2001). A genomic timescale for the origin of eukaryotes. *BMC Evolutionary Biology*, 1(1), 4. https://doi.org/10.1186/1471-2148-1-4

Houari, A., Picard, J., Habarou, H., Galas, L., Vaudry, H., Heim, V., & Di Martino, P. (2008). Rheology of biofilms formed at the surface of NF membranes in a drinking water production unit. *Biofouling*, 24(4), 235–240. https://doi.org/10.1080/08927010802023764

Huttenlochner, K., Davoudi, N., Schlegel, C., Bohley, M., Müller-Renno, C., Aurich, J. C., Ulber, R., & Ziegler, C. (2018). *Paracoccus seriniphilus* adhered on surfaces: Resistance of a seawater bacterium against shear forces under the influence of roughness, surface energy, and zeta potential of the surfaces. *Biointerphases*, 13(5), 51003. https://doi.org/10.1116/1.5049226

Kozuka, Y., Lu, Z., Masuda, T., Hara, S., Kasama, T., Miyake, R., Isu, N., & Takai, M. (2021). Evaluation of bacterial adhesion strength on phospholipid copolymer films with antibacterial ability using microfluidic shear devices. *Journal of Materials Chemistry. B*, 9(22), 4480–4487. https://doi.org/10.1039/d1tb00657f

Kuddus, M., Singh, P., Thomas, G., & Al-Hazimi, A. (2013). Recent developments in production and biotechnological applications of C-phycocyanin. *BioMed Research International*, 2013, 1–9. https://doi.org/10.1155/2013/742859

Law, K. Y. (2014). Definitions for hydrophilicity, hydrophobicity, and superhydrophobicity: Getting the basics right. *The Journal of Physical Chemistry Letters*, 5(4), 686–688. https://doi.org/10.1021/jz402762h

Li, T., Lin, G., Podola, B., & Melkonian, M. (2015). Continuous removal of zinc from wastewater and mine dump leachate by a microalgal biofilm PSBR. *Journal of Hazardous Materials*, 297, 112–118.

Li, X., Wei, Q., Tu, X., Zhu, Y., Chen, Y., Guo, L., Zhou, J., & Sun, H. (2016). Effects of nutrient loading on *Anabaena flos-aquae* biofilm: Biofilm growth and nutrient removals. *Water Science and Technology*, 74(2), 385–392. https://doi.org/10.2166/wst.2016.208

Lopez-Mila, B., Alves, P., Riedel, T., Dittrich, B., Mergulhão, F., & Rodriguez-Emmenegger, C. (2018). Effect of shear stress on the reduction of bacterial adhesion to antifouling polymers. *Bioinspiration & Biomimetics*, 13(6), 065001. https://doi.org/10.1088/1748-3190/aadcc2

Lupatini, A. L., Colla, L. M., Canan, C., & Colla, E. (2017). Potential application of microalga *Spirulina platensis* as a protein source. *Journal of the Science of Food and Agriculture*, 97(3), 724–732. https://doi.org/10.1002/jsfa.7987

Menter, F. R. (1992). Improved two-equation k-omega turbulence models for aerodynamic flows (No. NASA-TM-103975, A-92183, NAS 1.15:103975).

Murga, R., Stewart, P. S., & Daly, D. (1995). Quantitative analysis of biofilm thickness variability. *Biotechnology and Bioengineering*, 45(6), 503–510. https://doi.org/10.1002/bit.260450607

Murphy, T. E., & Berberoglu, H. (2014). Flux balancing of light and nutrients in a biofilm photobioreactor for maximizing photosynthetic productivity. *Biotechnology Progress*, 30(2), 348–359. https://doi.org/10.1002/btpr.1881

Nickzad, A., & Déziel, E. (2014). The involvement of rhamnolipids in microbial cell adhesion and biofilm development—An approach for control. *Letters in Applied Microbiology*, 58(5), 447–453. https://doi.org/10.1111/lam.12211

Ohashi, A., & Harada, H. (1994). Adhesion strength of biofilm developed in an attached-growth reactor. *Water Science and Technology*, 29(10–11), 281–288. https://doi.org/10.2166/wst.1994.0771

Ozkan, A., & Berberoglu, H. (2013). Adhesion of algal cells to surfaces. *Biofouling*, 29(4), 469–482. https://doi.org/10.1080/08927014.2013.782397

Sandal, I., Hong, W., Swords, W. E., & Inzana, T. J. (2007). Characterization and comparison of biofilm development by pathogenic and commensal isolates of *Histophilus somni*. *Journal of Bacteriology*, 189(22), 8179–8185. https://doi.org/10.1128/JB.00479-07

Scherer, K., Stiefelmaier, J., Strieth, D., Wahl, M., & Ulber, R. (2020). Development of a lightweight multi-skin sheet photobioreactor for future cultivation of phototrophic biofilms on facades. *Journal of Biotechnology*, 320, 28–35. https://doi.org/10.1016/j.jbiotec.2020.06.004

Schirrmeister, B. E., Gugger, M., & Donoghue, P. C. J. (2015). Cyanobacteria and the great oxidation event: Evidence from genes and fossils. *Palaeontology*, 58(5), 769–785. https://doi.org/10.1111/pala.12178

Schlegel, C. (2015). Produktive Biofilme auf mikrostrukturierten Metalloberflächen (Dissertation).

Schmidt, T., & Just, L. (2006). Device and method for the cultivation and production of biological material in a nutrient mist. WO2007068467A1.

Song, F., Koo, H., & Ren, D. (2015). Effects of material properties on bacterial adhesion and biofilm formation. *Journal of Dental Research*, 94(8), 1027–1034. https://doi.org/10.1177/0022034515587690

Stanier, R. Y., Deruelles, J., Rippka, R., Herdman, M., & Waterbury, J. B. (1979). Generic assignments, strain histories and properties of pure cultures of Cyanobacteria. *Microbiology*, 111(1), 1–61. https://doi.org/10.1099/00221287-111-1-1

Strieth, D., Schwing, J., Kuhne, S., Lakatos, M., Muffler, K., & Ulber, R. (2017). A semi-continuous process based on an ePBR for the production of EPS using *Trichocoleus sociatus*. *Journal of Biotechnology*, 256, 6–12. https://doi.org/10.1016/j.jbiotec.2017.06.1205

Strieth, D., Stiefelmaier, J., Wrabl, B., Schwing, J., Schmeckebier, A., Di Nonno, S., & Ulber, R. (2020). A new strategy for a combined isolation of EPS and pigments from Cyanobacteria. *Journal of Applied Phycology*, 32, 1729. https://doi.org/10.1007/s10811-020-02063-x

Strieth, D., Weber, A., Robert, J., Stiefelmaier, J., Kollmen, J., Volkmar, M., Lakatos, M., Jordan, V., Muffler, K., & Ulber, R. (2021). Characterization of an aerosol-based photobioreactor for cultivation of phototrophic biofilms. *Life*, 11(10), 1046. https://doi.org/10.3390/life11101046

Stuart, R. K., Mayali, X., Lee, J. Z., Craig Everroad, R., Hwang, M., Bebout, B. M., Weber, P. K., Pett-Ridge, J., & Thelen, M. P. (2016). Cyanobacterial reuse of extracellular organic carbon in microbial mats. *The ISME Journal*, 10(5), 1240–1251. https://doi.org/10.1038/ismej.2015.180

Swain, S. S., Paidesetty, S. K., & Padhy, R. N. (2017). Antibacterial, antifungal and antimycobacterial compounds from Cyanobacteria. *Biomedicine & Pharmacotherapy=Biomedecine & Pharmacotherapie*, 90, 760–776. https://doi.org/10.1016/j.biopha.2017.04.030

Sweity, A., Ying, W., Ali-Shtayeh, M. S., Yang, F., Bick, A., Oron, G., & Herzberg, M. (2011). Relation between EPS adherence, viscoelastic properties, and MBR operation: Biofouling study with QCM-D. *Water Research*, 45(19), 6430–6440. https://doi.org/10.1016/j.watres.2011.09.038

Tamaru, Y., Takani, Y., Yoshida, T., & Sakamoto, T. (2005). Crucial role of extracellular polysaccharides in desiccation and freezing tolerance in the terrestrial cyanobacterium *Nostoc commune*. *Applied and Environmental Microbiology*, 71(11), 7327–7333. https://doi.org/10.1128/AEM.71.11.7327-7333.2005

Tolker-Nielsen, T. (2015). Biofilm development. *Microbiology Spectrum*, 3(2), MB-0001-2014. https://doi.org/10.1128/microbiolspec.MB-0001-2014

Towler, B. W., Rupp, C. J., Cunningham, A. B., & Stoodley, P. (2003). Viscoelastic properties of a mixed culture biofilm from rheometer creep analysis. *Biofouling*, 19(5), 279–285. https://doi.org/10.1080/0892701031000152470

Wigneswaran, V., Nielsen, K. F., Sternberg, C., Jensen, P. R., Folkesson, A., & Jelsbak, L. (2016). Biofilm as a production platform for heterologous production of rhamnolipids by the non-pathogenic strain *Pseudomonas putida* KT2440. *Microbial Cell Factories*, 15(1), 181. https://doi.org/10.1186/s12934-016-0581-9

SUPPORTING INFORMATION

Additional supporting information can be found online in the Supporting Information section at the end of this article.